AZIMUTHAL ANGULAR DECORRELATION OF JETS AT FUTURE HIGH-ENERGY COLLIDERS*

İ. Hoş†, H. Saygin‡, S. Kuday§

Istanbul Aydın University
Application and Research Center For Advanced Studies
34295 Istanbul, Turkey

(Received September 5, 2018; accepted January 10, 2019)

The azimuthal angular decorrelation that is relevant to small-x QCD physics is studied in this paper to show the BFKL effect with a recent event generator. Events are generated at $\sqrt{s} = 100$ TeV with proton–proton collisions and jets that are reconstructed by the anti-k_{T} algorithm ($R = 0.7$) with $p_{\mathrm{T}} > 35$ GeV and in the rapidity range of $|y| < 6$ are selected for the study. The azimuthal-angle difference between Mueller–Navelet jets ($\Delta\Phi$) in the rapidity separation (Δy) up to 12 is analysed. The distributions of $\langle \cos n(\pi - \Delta\Phi) \rangle$ for $n = 1, 2, 3$ and their ratios are also presented as a function of Δy.

DOI:10.5506/APhysPolB.50.149

1. Introduction

The strong interaction between quarks and gluons, called partons, are defined by the theory of Quantum Chromodynamics (QCD). According to QCD, quarks carry colour charges (blue, red and green) and cannot be observed as free particles but in colourless states. This behaviour is named as confinement. To study partons experimentally, one needs to consider jets described by QCD in terms of pp scattering.

The momentum distribution functions of partons within the proton are described by the evaluation equations, when running coupling as one moves from one momentum scale to another. One of these evolution equations is BFKL (Balitsky, Fadin, Kuraev, Lipatov) [1–3] which describes the dependence on x, the parton momentum fraction. BFKL equations require strong

* Funded by SCOAP[3] under Creative Commons License, CC-BY 4.0.

† ilknurhos@aydin.edu.tr
‡ hasansaygin@aydin.edu.tr
§ sinankuday@aydin.edu.tr

ordering of fractional momentum. An ideal observable to study sensitivity of low-x QCD evolution and a test of BFKL is the distribution of azimuthal angle between two jets in the same event. At the leading order calculations, two jets are back-to-back in xy-plane and perfectly correlated. However, when the energy of collision increases, the correlation of two jets breaks down by the emission of an extra jet, and the two selected jets are no longer back-to-back in the xy-plane.

At Fermilab Tevatron, the studies of BFKL effect are performed at $\sqrt{s} =$ 1.8 TeV, 1800 and 630 GeV by D0 experiment [4, 5]. At both studies, $\Delta\eta$ is selected up to 6, which could limit the observation of decorrelation effect.

The experiments at the LHC provide larger rapidity separation and higher center-of-mass energy for the studies. The publication from the ATLAS Collaboration [6] is performed at $\sqrt{s} = 7$ TeV using jets with $p_{\mathrm{T}} > 20$ GeV and rapidity separation of $|\Delta y| < 6$, and concludes that PYTHIA [24] and Herwig [27] give the best description of data as a function of mean transverse momentum, $\bar{p}_{\mathrm{T}}$, while PYTHIA gives the best description of data as a function of Δy. CMS publications [7, 8] report the measurements at 7 TeV and with jets $p_{\mathrm{T}} > 35$ GeV and in the rapidity region of $|y| < 4.7$. These publications indicate that one can observe the BFKL effect at higher center-of-mass energies.

There are also some phenomenological studies performed at the kinematical conditions of the LHC. In [9] and [10], authors performed NLL BFKL calculations with MN jets. References [11, 13] and [12] are focused on NLA (next to leading approximation) BFKL approach at MN jet production at the LHC energies. Reference [12] shows the results of kinematics of MN jets for asymmetric cuts for the transverse momentum. The results of Ref. [13] indicate the decrease of $\langle\cos(\Phi)\rangle$ with increasing rapidity. However, in contrast, Ref. [14] shows no decorreleation rise for increasing rapidity and suggests that differences between BFKL and DGLAP cannot be observed with MN jet production.

Recently, new projects based on higher-collision energies have been considering to extend the search performed at the LHC. As one of these projects, Future Circular Collider (FCC) [15, 16] is planned to be built on 80–100 km tunnel to reach the 100 TeV collision energy. FCC is hosted by CERN and planned to develop three accelerator facilities: FCC-hh, FCC-he and FCC-ee. Another future collider project is Circular Electron Positron Collider (CEPC) with the design of Super Proton–Proton Collider (SPPC) [17, 18]. The CEPC-SPPC is planned to have baseline of 100 km circumference and to reach the center-of-mass energy of 100 TeV. Since there is no available data at 100 TeV, to see the BFKL effect at such center-of-mass energies, one can simulate hard QCD events and use jet reconstruction algorithms to investigate kinematic distributions.

2. Small-x physics

According to Quark–Parton Model, protons are made of point-like particles, called partons. Thus, when two hadrons collide, quarks and gluons inside incoming hadrons interact with each other, indeed. The decrease of the dependence of the structure functions on energy scale Q^2 is predicted by increasing center-of-mass energies. Later, structure functions become the function of x alone. The probability of finding a parton carrying a fraction x of the momentum of the proton is defined by parton distribution functions (PDFs). The change in parton distributions with variation in momentum scale is described by evolution equations. The BFKL evolution equation becomes valid at small-x values. BFKL allows the resummation of terms with $(\alpha_s \log(\frac{1}{x}))^n$ (where α_s is strong coupling), so it is valid at $\log\left(\frac{Q^2}{Q_0^2}\right) \ll \log\left(\frac{1}{x}\right)$.

Jets are particle sprays emitted from hadron–hadron collisions. The measurement of jet shapes allows one to study the transition between a parton, coming from hard scattering, and a hadron, observed experimentally. Mueller–Navelet jets (MN jets) [19] are produced during hadron–hadron collisions at high energies. These jets carry the longitudinal momentum fraction of their parent hadrons. Thus, each jet is closed to its parent hadron and that causes a large rapidity separation between jets. Such a process allows to study the BFKL evidence. During the collision, dijets are correlated and can be observed back-to-back or with different angles. Back-to-back jets are balanced in transfer momentum and perfectly correlated. However, when an extra jet is emitted in such a process, the decorrelation begins to appear and break-down of back-to-back topology increases.

There are three observables that can show the effect of BFKL. One is azimuthal angle between MN jets ($\Delta\Phi$) with respect to rapidity separation between jets as suggested at [20]. If jets are highly correlated and back-to-back, there should be a sharp peak in the distribution of $\Delta\Phi$. However, by increasing rapidity separation between jets, the $\Delta\Phi$ peak decreases and distribution becomes wider. The second observable is average cosine value of $\Delta\Phi$ ($\langle\cos(\pi - \Delta\Phi)\rangle$) [4, 21]. When jets are back-to-back and perfectly correlated, one should expect a flat distribution at 1 in the plot of $\langle\cos(\pi - \Delta\Phi)\rangle$. When decorrelation arises with extra jet emission, the $\langle\cos(\pi - \Delta\Phi)\rangle$ value starts to decrease with increasing rapidity separation. The third observable can be a ratio of $\langle\cos n(\pi - \Delta\Phi)\rangle$ for different n values as proposed in [22, 23]. That plot shows also a clear change of $\langle\cos(\pi - \Delta\Phi)\rangle$.

3. Event and jet selection

PYTHIA 8 [24] is used to generate the hard QCD events with proton–proton collisions at $\sqrt{s} = 100$ TeV. 30×10^6 events are generated and during the generation of events, FastJet [25] is used to reconstruct the jets by anti-k_T [26] jet algorithm with cone radius of 0.7. As the preselection criteria, events with at least two jets are used and jets are required to pass p_T cut of 10 GeV and to be in the rapidity region of $|y| < 7$.

In the analysis, the following criteria are applied to select the jets:

— p_T higher than 35 GeV;

— in the rapidity region of $|y| < 6$;

— assign rapidity ordering of jets for each event, choose the jets with highest rapidity and lowest rapity value, and name them most forward jet and most backward jet, respectively.

By that selection, in each event, these two jets would have largest rapidity separation and can be named as Mueller–Navelet jets. The control plots are produced to see the effect of selection criteria. Figure 1 shows p_T distributions of forward and backward jets which have p_T higher than 35 GeV. It is clear that during the analysis, both most forward and most backward jets having $p_T > 35$ GeV are used. In figure 2, rapidity of MN jets is plotted, while phi distribution is shown in figure 3. These two figures show that most of the jets are in back-to-back in xy-plane.

The number of events and number of jets before and after cuts are presented in Table I. Table II shows the number of jets at each $\Delta\Phi$ distribution at $\sqrt{s} = 100$ TeV. The number of jets decreases with large rapidity separation.

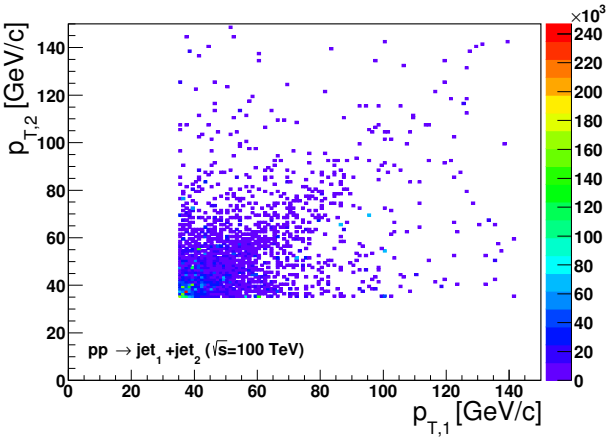

Fig. 1. Forward jet p_T *versus* backward jet p_T.

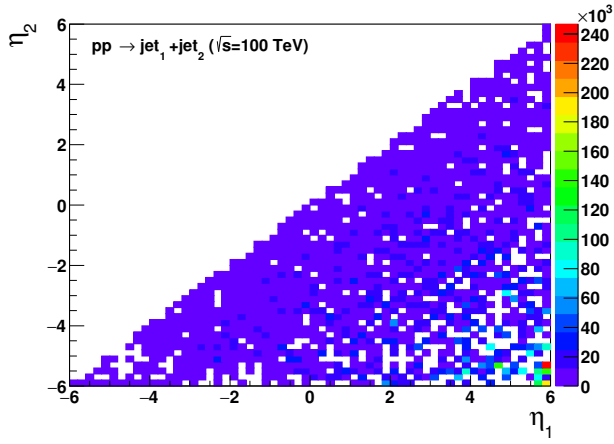

Fig. 2. Forward jet rapidity *versus* backward jet rapidity.

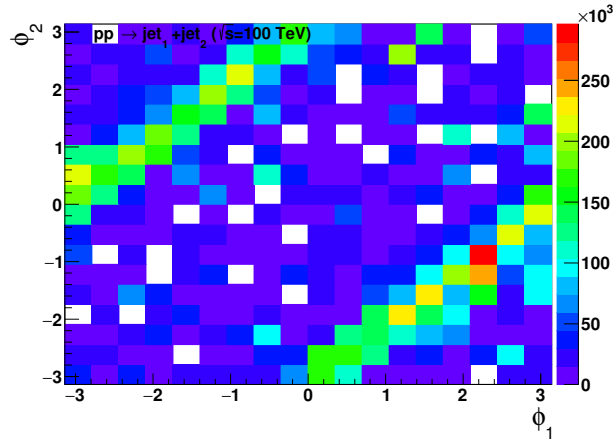

Fig. 3. Forward jet phi *versus* backward jet phi.

TABLE I

Number of events and number of jets before and after cuts at $\sqrt{s} = 100$ TeV.

$\sqrt{s} = 100$ TeV	Before cuts	Events with at least 2 jets and jet $p_{\mathrm{T}} > 35$ GeV	After MN jets selection criteria
Number of events	3e+07	4.3733e+06	3442
Number of jets	1.92805e+12	3.28932e+10	1.41547e+07

TABLE II

Number of jets at each $\Delta\Phi$ distribution at $\sqrt{s} = 100$ TeV.

	$\lvert\Delta y\rvert < 3$	$3 < \lvert\Delta y\rvert < 6$	$6 < \lvert\Delta y\rvert < 9$	$9 < \lvert\Delta y\rvert < 12$
Number of jets	3427680	4465153	3353053	2904755

4. Analysis

After being sure about selection of MN jets, the result plots are produced. The first observable to see the signs of BFKL effect, the azimuthal-angle difference between MN jets ($\Delta\Phi$) as a function of the rapidity separation of MN jets, is shown in figure 4. As described in previous section, the decorrelation will rise by increasing rapidity separation between jets. To see the effect clearly, the distribution is plotted for four rapidity separations: $|\Delta y| < 3$, $3 < |\Delta y| < 6$, $6 < |\Delta y| < 9$, and $9 < |\Delta y| < 12$. If one checks first binning of the histogram, then can see clearly that $|\Delta y| < 3$ is in the top, while in the last binnings it is in the bottom and $9 < |\Delta y| < 12$ appears in the top. That shows that with increasing rapidity between jets, the peak of $\Delta\Phi$ distribution decreases and the distribution becomes wider comparing to the distributions with narrower Δy.

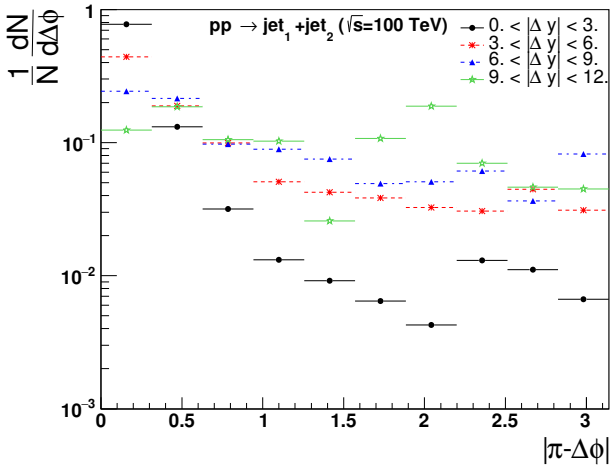

Fig. 4. The azimuthal-angle difference between MN jets ($\Delta\Phi$) in the rapidity of $|\Delta y| < 3$, $3 < |\Delta y| < 6$, $6 < |\Delta y| < 9$ and $9 < |\Delta y| < 12$ at $\sqrt{s} = 100$ TeV.

The second observable to see the BFKL effect, $\langle\cos(\pi - \Delta\Phi)\rangle$ distribution between MN jets, is shown in figure 5. $\langle\cos n(\pi - \Delta\Phi)\rangle$ is presented for $n = 1, 2$ and 3 with different line colors. The distribution starts around 1

and then decreases for larger rapidity separation. When n increases, the change in the distribution becomes more significant. There are observed some statistical fluctuations in the distributions.

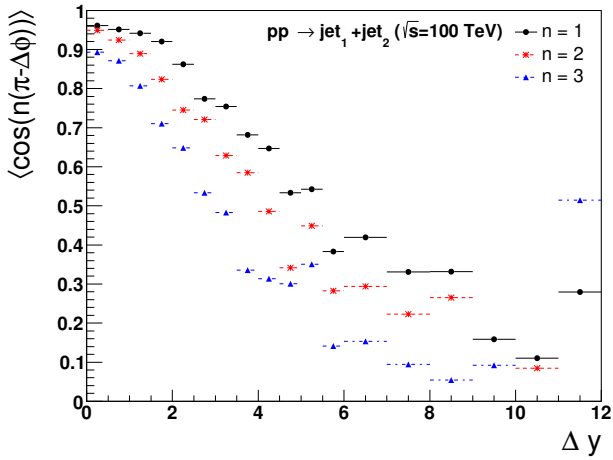

Fig. 5. (Colour on-line) $\langle\cos(\pi-\Delta\Phi)\rangle$, $\langle\cos 2(\pi-\Delta\Phi)\rangle$ and $\langle\cos 3(\pi-\Delta\Phi)\rangle$ as a function of Δy at $\sqrt{s}=100$ TeV.

Figure 6 shows the ratio of $\langle\cos 2(\pi-\Delta\Phi)\rangle$ to $\langle\cos(\pi-\Delta\Phi)\rangle$ ($\frac{C_2}{C_1}$, left plot) and $\langle\cos 3(\pi-\Delta\Phi)\rangle$ to $\langle\cos 2(\pi-\Delta\Phi)\rangle$ ($\frac{C_3}{C_2}$, right plot) as a function of the rapidity separation Δy. The values of ratio plots for each bin are listed in Table III. Except the bins with low statistics, the general behaviour of distribution is decreasing as a function of Δy and the values of very forward bins become negative.

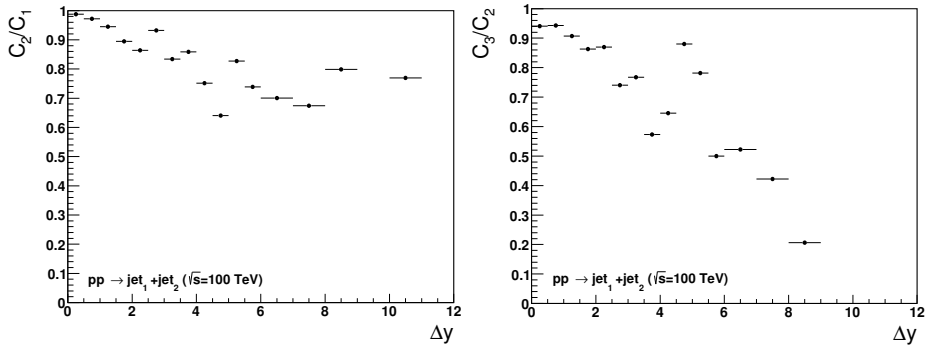

Fig. 6. Ratio of average cosine $\frac{C_2}{C_1}$ (left) and $\frac{C_3}{C_2}$ (right) as a function of Δy at $\sqrt{s}=100$ TeV.

TABLE III

Values of $\frac{C_2}{C_1}$ and $\frac{C_3}{C_2}$ corresponding to figure 6.

Δy	$\frac{C_2}{C_1}$	$\frac{C_3}{C_2}$
0–0.5	0.987901	0.9406833
0.5–1	0.9718233	0.9427983
1–1.5	0.944672	0.9067067
1.5–2	0.8946949	0.8627438
2–2.5	0.8641118	0.8700755
2.5–3	0.9320614	0.7401573
3–3.5	0.8336877	0.7674307
3.5–4	0.8583582	0.5731944
4–4.5	0.7515884	0.6458528
4.5–5	0.6404151	0.8799939
5–5.5	0.8274014	0.7812541
5.5–6	0.7383662	0.5002056
6–7	0.7004598	0.5225553
7–8	0.6741877	0.4224949
8–9	0.7990478	0.2063604
9–10	−0.7937955	−0.7309967
10–11	0.7692262	−0.6317346
11–12	−0.05910809	−31.19034

5. Conclusion

In the analysis, we have showed a significant difference between the kinematic distributions of MN jets that are selected to have largest rapidity separation with $p_{\mathrm{T}} > 35$ GeV at $\sqrt{s} = 100$ TeV using PYTHIA 8 event generator and FastJet clustering algorithm which are considered as one of the most realistic and updated tools in data analysis. In figure 4, one can see that the peak of azimuthal-angle distributions of MN jets is decreasing with selected rapidity regions (Δy) up to 12 and getting wider by the function of Δy. We have found that the distributions of jets for rapidity regions of $|\Delta y| < 3$, $3 < |\Delta y| < 6$, $6 < |\Delta y| < 9$, $9 < |\Delta y| < 12$ are 24.2%, 31.6%, 23.7% and 20.6%, respectively. The average cosine value of $\Delta\Phi$ also decreases with the increasing Δy in figure 5. The same effect can be seen in the ratio plots of $\langle \cos n(\pi - \Delta\Phi) \rangle$ for $n = 1, 2, 3$ except the bins suffering from low statistics. This effect in average cosine and ratio plots is also predicted by [13]. However, previous studies described in Introduction, some of which show the same and some opposite effect, are performed at the LHC energies.

In conclusion, with increasing center-of-mass energies, the observables of BFKL effects become significant for jet-based analysis particularly in the forward regions of detectors and can only be justified by collected data at future high-energy colliders such as FCC and CEPC-SPPC. Therefore, one should consider the BFKL evolution equation and parton momentum fraction (x) dependency in the parton distribution functions in the analysis of experimental data in order to achieve more accurate results from jet-based analyses.

REFERENCES

[1] E.A. Kuraev, L.N. Lipatov, V.S. Fadin, *Sov. Phys. JETP* **44**, 443 (1976).

[2] E.A. Kuraev, L.N. Lipatov, V.S. Fadin, *Sov. Phys. JETP* **45**, 199 (1977).

[3] I.I. Balitsky, L.N. Lipatov, *Sov. J. Nucl. Phys.* **28**, 822 (1978).

[4] D0 Collaboration, *Phys. Rev. Lett.* **77**, 595 (1996) [arXiv:hep-ex/9603010].

[5] D0 Collaboration, *Phys. Rev. Lett.* **84**, 5722 (2000) [arXiv:hep-ex/9912032].

[6] ATLAS Collaboration, *J. High Energy Phys.* **1109**, 053 (2011) [arXiv:1107.1641 [hep-ex]].

[7] CMS Collaboration, *Eur. Phys. J. C* **72**, 2216 (2012) [arXiv:1204.0696 [hep-ex]].

[8] CMS Collaboration, *J. High Energy Phys.* **1608**, 139 (2016).

[9] B. Ducloue, L. Szymanowski, S. Wallon, *J. High Energy Phys.* **1305**, 096 (2013).

[10] B. Ducloue, L. Szymanowski, S. Wallon, *Phys. Rev. Lett.* **112**, 082003 (2014).

[11] F. Caporale, D.Yu. Ivanov, B. Murdaca, A. Papa, *Eur. Phys. J. C* **74**, 3084 (2014) [*Erratum ibid.* **75**, 535 (2015)].

[12] F.G. Celiberto, D.Yu. Ivanov, B. Murdaca, A. Papa, *Eur. Phys. J. C* **75**, 292 (2015).

[13] F. Caporale, D.Yu. Ivanov, B. Murdaca, A. Papa, *Nucl. Phys. B* **877**, 73 (2013).

[14] D. Colferai, F. Schwennsen, L. Szymanowski, S. Wallon, *J. High Energy Phys.* **1012**, 026 (2010).

[15] The Future Circular Collider Study Group, Kickoff Meeting, February 12–15, 2014, University of Geneva, Switzerland, https://indico.cern.ch/event/282344/. More information is available on the FCC Web site: http://cern.ch/fcc

[16] A. Ball *et al.*, Future Circular Collider Study Hadron Collider Parameter *s*, FCC-ACC-SPC-0001, 2014.

[17] The CEPC-SPPC Study Group, CEPC-SPPC Preliminary Conceptual Design Report, Volume II-Accelerator, IHEP-AC-2015-01, March 2015.

[18] J. Gao, *Int. J. Mod. Phys. A* **32**, 1746003 (2017).

[19] A.H. Mueller, H. Navelet, *Nucl. Phys. B* **282**, 727 (1987).

[20] V. Del Duca, C.R. Schmidt, *Phys. Rev. D* **49**, 4510 (1994).

[21] C.L. Kim, A Study of the Azimuthal Decorrelation Between Jets with Large Rapidity Separation, FERMILAB-THESIS-1996-30, 1996.

[22] A. Sabio Vera, *Nucl. Phys. B* **746**, 1 (2006) [arXiv:hep-ph/0602250].

[23] A. Sabio Vera, F. Schwennsen, *Nucl. Phys. B* **776**, 170 (2007) [arXiv:hep-ph/0702158].

[24] T. Sjöstrand *et al.*, *Comput. Phys. Commun.* **191**, 159 (2015).

[25] M. Cacciari, G.P. Salam, G. Soyez, *Eur. Phys. J. C* **72**, 1896 (2012).

[26] M. Cacciari, G.P. Salam, G. Soyez, *J. High Energy Phys.* **0804**, 063 (2008) [arXiv:0802.1189 [hep-ph]].

[27] S. Gieseke *et al.*, arXiv:1102.1672 [hep-ph].